# Time-Resolved FT-Infrared Spectroscopy of Visible Light-Induced Alkene Oxidation by $O_2$ in a Zeolite

**Sergey Vasenkov and Heinz Frei***

*Physical Biosciences Division, MS Calvin Laboratory, Lawrence Berkeley National Laboratory, University of California, Berkeley, California 94720*

*Received: February 5, 1998; In Final Form: May 8, 1998*

The visible light-induced reaction between 2,3-dimethyl-2-butene and $O_2$ in zeolite NaY at −100 °C was recorded on the millisecond time scale by rapid scan FT-infrared spectroscopy. The experiment revealed the growth of the sole product, 2,3-dimethyl-3-hydroperoxy-1-butene, during a 150 ms photolysis pulse. Since this duration is short compared to the time scale estimated for cage-to-cage diffusion of the product, it allowed us to determine the number of cages participating in the reaction induced by the pulse. On the basis of this measurement and a comparison of product yields in pulsed and continuous irradiation experiments, we estimate that at a minimum 1% of all NaY supercages participate in the photoreaction. This is 1−3 orders of magnitude larger than the concentration of any defect sites (Lewis acid, radical sites) that might be present in NaY zeolite. This confirms that the sole physical property of the zeolite cage, namely the high electrostatic field in the vicinity of the alkali ions, is responsible for the visible light-induced olefin oxidation.

## I. Introduction

In recent photochemical work on hydrocarbon oxidation by $O_2$ in zeolites, we have found that small alkenes, alkanes, or alkylbenzenes can be partially oxidized under visible light with very high selectivity.[1] The primary photoproduct detected by in situ FT-infrared spectroscopy is the corresponding allyl, alkyl, or benzyl hydroperoxide. Final oxidation products of these reactions, which were conducted on mixtures of hydrocarbon and $O_2$ gas loaded into alkali or alkaline-earth zeolite Y or L, are the corresponding aldehyde or ketone. Exceptions are systems such as 2,3-dimethyl-2-butene or isobutane whose hydroperoxide product does not feature an H at the α carbon, preventing spontaneous dehydration to form a carbonyl compound.[1b,e] Products of these partial oxidations are of commercial importance, and the high selectivity is a unique aspect of the method. To expand such visible light-induced reactions in zeolites to new synthesis, a firm understanding of the mechanism is essential. This motivated us to employ time-resolved FT-infrared spectroscopy as a tool for gaining mechanistic insight not accessible in our previous studies using static FT-IR spectroscopy.

UV−visible spectroscopy of alkali and alkaline-earth zeolite Y loaded with alkane (alkene, arene) and $O_2$ revealed a visible absorption tail attributed to the hydrocarbon·$O_2$ contact charge-transfer transition.[2,3] This assignment is based on the observed increase of the absorption threshold with the ionization potential of the hydrocarbon. UV charge-transfer bands of alkane, alkene, or arene·$O_2$ contact complexes are well-known from studies in the high-pressure $O_2$ gas phase and $O_2$-saturated solution.[4−6] Further strong evidence for the charge-transfer assignment is the dependence of the absorption onset on the magnitude of the electrostatic field in the vicinity of exchangeable cations in the zeolite cage.[2] These fields lie at the origin of the mild oxidation method. In the case of NaY or BaY, for example, the zeolites most frequently used in our experiments, there are 3−4 cations located in each supercage.[7] The wall of the cage carries a formal negative charge of 7 which resides on the framework oxygens. The electric shielding of the cations in the supercage by the wall oxygens is poor, resulting in high electrostatic fields around the cations. There is extensive experimental evidence for these electrostatic fields in cation-exchanged zeolites from infrared[8−11] and ESR spectroscopy[12,13] of small guest molecules, from electron densities determined by X-ray measurements,[14] and from heat of adsorptions of rare gases.[15] Model and ab initio calculations confirm these results.[16−18] The interaction of the high electrostatic field (NaY, 0.3 V Å$^{-1}$; BaY, 0.9 V Å$^{-1}$)[19] with the large dipole generated upon excitation of the hydrocarbon·$O_2$ pair to the charge-transfer state (about 15 D) leads to a stabilization of the state by 1.5−3 eV for pairs oriented parallel to the field. The result is a very large red shift of the absorption from the UV into the visible region. It is excitation of this hydrocarbon·$O_2$ charge-transfer state, rendered accessible to visible light by the presence of high electrostatic fields in the zeolite, that is responsible for the observed photochemistry.

While the hydrocarbon·$O_2$ charge-transfer absorption is well established as the chromophore initiating the photoreaction, direct evidence is still lacking that electrostatic and steric properties are really the only zeolite properties that play a role in the reaction mechanism. We have no spectroscopic evidence for other properties of the zeolite materials used in our work that may play a role, such as Lewis acid sites or radical defects, as described in a previous report.[1f] Nevertheless, while not detectable spectroscopically, a small concentration of such sites might still play a role in the hydrocarbon oxidation mechanism if turnover in those zeolite cages is sufficiently fast. If it were possible to monitor the growth of the primary photoproduct on a time scale short compared to cage-to-cage diffusion of products or reactants, we would be able to determine whether turnover at a small number of defect sites plays a role. In this paper, we report a millisecond FT-infrared study of the visible light-induced reaction of 2,3-dimethyl-2-butene (DMB) and $O_2$ in zeolite NaY at 173 K which allowed us to address this question (Scheme 1). This olefin + $O_2$ system was chosen because it

S1089-5647(98)01035-9 CCC: $15.00 
Published on Web 06/25/1998

**SCHEME 1**

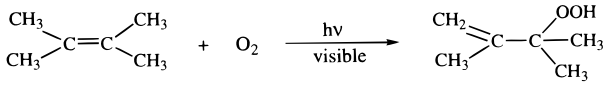


has the strongest charge-transfer absorption in the visible and the fastest photochemical rate of the hydrocarbons studied thus far.[2]

## II. Experimental Section

Self-supporting wafers of 4−7 mg of zeolite NaY (LZ-Y52, Aldrich Chemical Co., Lot #12929CN) were pressed and mounted inside a miniature infrared vacuum cell described in previous work.[1] The infrared cell was mounted inside a variable temperature vacuum system (Oxford cryostat, model DN1724) with a temperature range from 77 to 473 K. The zeolite pellet was dehydrated at 200 °C for 12−15 h under high vacuum (turbomolecular pump, model Varian V-60), resulting in a residual $H_2O$ level of one molecule per three supercages.[1i] 2,3-Dimethyl-2-butene (DMB) was loaded from the gas phase (0.8 Torr) into the zeolite held at 223 K. Oxygen (800 Torr) or nitrogen gas (125 Torr) was added after the hydrocarbon loading. This resulted in 1−2 olefins per supercage and about one $O_2$ or $N_2$ molecule per three supercages. Time-resolved photolysis experiments were conducted at a zeolite temperature of 173 K.

Time-resolved FT-infrared spectra were recorded by the rapid scan method using a Bruker model IFS88 FT-IR spectrometer.[20] Infrared detectors used were a HgCdTe detector (Kolmar Technologies, model KMPV11-1-J2) for spectroscopy below 2000 $cm^{-1}$ and an InSb detector (EG&G Judson, model J100) for the region 4000−2000 $cm^{-1}$. Folding limits were tailored to spectral regions of interest for maximum sensitivity. For the fingerprint region, the folding limits were 2250 and 1130 $cm^{-1}$, requiring an infrared filter (Optical Coating Laboratory, model #W07100-11X) for blocking of light outside these limits. (Light below 1200 $cm^{-1}$ was cut off by the zeolite framework absorption.) Folding limits for recording with the InSb detector were 3700 and 2300 $cm^{-1}$, requiring an Optical Coating Laboratory filter, model #W03506-6. Reaction was initiated by a visible light pulse from an Ar ion laser (Coherent, model Innova 90-6) equipped with a mechanical shutter (UniBlitz, model D122). The emission wavelengths of the Ar ion laser were 514 and 488 nm "all lines" (500 mW total power), and the pulse width of the mechanical shutter was 150 ms. A small prism (1 cm edge-to-edge) was used to align the photolysis beam collinear with the infrared probe beam. To prevent photolysis light from entering the detector or interferometer compartment, the ports to both compartments were protected each by a 2 in. germanium plate with a dielectric coating that maximized the infrared transmittance (95%, International Scientific).

Rapid scan measurements were conducted with a mirror velocity of 160 kHz and a spectral resolution of 4 $cm^{-1}$ (2200−1200 $cm^{-1}$) or 16 $cm^{-1}$ (3700−2300 $cm^{-1}$). This resulted in a single interferogram scan time of 130 ms (2200−1200 $cm^{-1}$) or 60 ms (3700−2300 $cm^{-1}$). The mirror performed 50 such scans after each photolysis pulse in the 2200−1200 $cm^{-1}$ experiment or 100 scans when running experiments in the 3700−2300 $cm^{-1}$ region. The dark period between laser pulses was about 6 s. Four consecutive 130 ms scans or eight scans of 60 ms duration were automatically averaged and the results stored. Hence, up to 12 averaged interferograms could be obtained after each laser pulse, furnishing 12 single beam spectra upon Fourier transformation. To optimize the use of computer memory, only averaged interferograms at three different time delays were digitized and processed. A typical experiment consisted of recording of the data of about 100 laser pulses. Start of interferogram acquisition following a laser pulse was triggered by an optical pulse diverted from the laser beam (silicon photodiode, EG&G model SGD-444). To ensure that the time delay between laser pulse and start of interferogram is exactly the same after each pulse, the shutter was triggered by a TTL pulse from the FT-IR instrument coincident with a forward turn of the moving interferometer mirror. These TTL pulses were sent through a home-built rate divider before entering the shutter driver in order to discriminate all pulses until recording of all interferograms was completed, resulting in a laser repetition rate of around $^1/_6$ Hz.

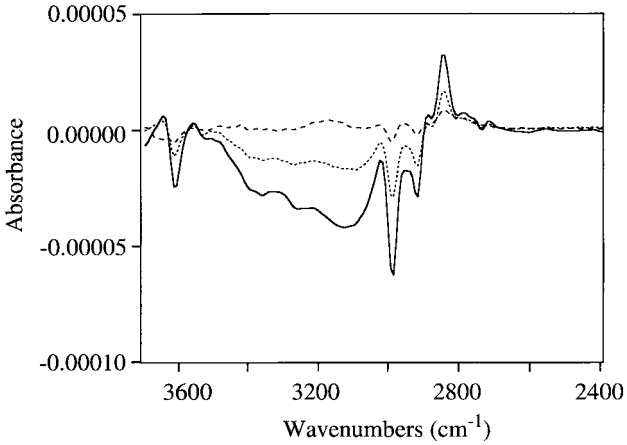


**Figure 1.** Rapid scan FT-IR spectra of the laser-induced DMB + $O_2$ reaction in NaY at 173 K. Time delays are 330 ms (solid line), 1280 ms (dotted line), and 2760 ms (dashed line). The result represents the average of 1040 laser pulses.

Final time-resolved spectra for a desired delay after the photolysis laser pulse were obtained by ratioing the corresponding stored single beam spectrum (one of the three recorded averages after each pulse) against the single beam spectrum taken just before the pulse. These ratioed spectra were then averaged. Calculations were carried out with a Macro program executed within the Bruker OPUS program.

2,3-Dimethyl-2-butene (Aldrich, 99%) was vacuum-distilled before use. Oxygen and nitrogen gas (Air Products, 99.997%) were used as received.

## III. Results and Discussion

**1. Thermal Effect.** Rapid scan absorbance spectra of the DMB + $O_2$ photoreaction in the region 3700−2400 $cm^{-1}$ taken 330, 1280, and 2760 ms after the laser pulse are shown in Figure 1. The spectra are the result of averaging data from 1040 laser pulses (10 consecutive experiments). The delay times refer to the separation between the center of the 150 ms excitation pulse and the center of the first, third, and sixth spectrum (average of eight scans) recorded after the pulse. For the 330 and 1280 ms spectra, amplitudes are negative in most regions where the photoproduct, 2,3-dimethyl-3-hydroperoxy-1-butene, absorbs. The most prominent feature of the product is the broad OH stretching absorption with a peak at 3150 $cm^{-1}$.[1b] It shows up as a negative band in the first two traces of Figure 1. The negative amplitude vanishes within a few seconds after the laser pulse as can be seen from the 2760 ms spectrum, which shows a small growth around 3200 $cm^{-1}$. Such negative features with a recovery time of a few seconds are characteristic of a small thermal effect induced by the laser excitation pulse. We have

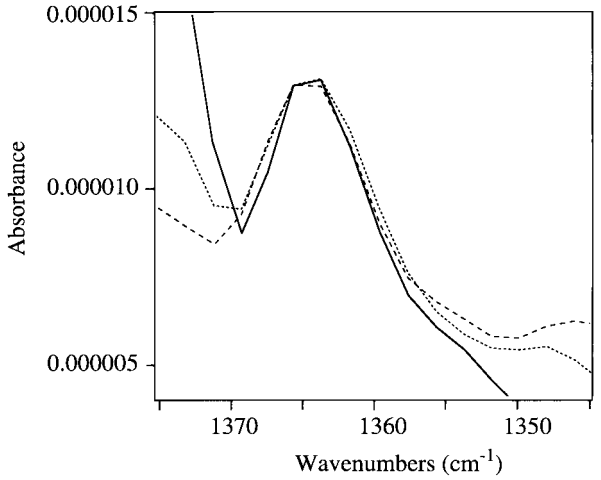


**Figure 2.** Rapid scan FT-IR spectra of the 1365 $cm^{-1}$ allyl hydroperoxide product absorption recorded 360 ms (solid line), 1360 ms (dotted line), and 2840 ms (dashed line) after the photolysis pulse. The signal change above 1370 $cm^{-1}$ is due to the thermal effect on the intense DMB reactant absorption at 1385 $cm^{-1}$.

described this effect, which obscures the product absorbance growth initiated by the laser pulse, in our previous work on UV excitation of a quinone molecule in zeolite NaY.[21] Comparison with static infrared spectra of 2,3-dimethyl-3-hydroperoxy-1-butene recorded at different zeolite temperatures indicates that the transient thermal effect in the pulsed laser experiment is 1−2 K. While it is highly reproducible for the OH stretching mode, this is not the case for the product and reactant (DMB) absorptions between 3000 and 2800 $cm^{-1}$. The thermal effect on the much stronger DMB reactant bands obscures the behavior of the hydroperoxide CH absorptions, which is compounded by the fact that the spectral resolution of 16 $cm^{-1}$ is insufficient to resolve reactant and product absorptions completely.

It is worth noting that the baseline of the transient spectra is not affected by the thermal effect (Figure 1). Since the scattering of light in the 2000−4000 $cm^{-1}$ region is even stronger than the absorption by the hydroperoxide product, any change in the refractive index of the zeolite pellet would have resulted in a significant baseline change. (According to the theory for particles smaller than the probe wavelength, change of the refractive index leads to comparable changes in scattering and absorption.[22]) The absence of any change of the baseline implies that the refractive index of the NaY crystallites is not affected by the laser irradiation pulse. The most probable origin of the thermal effect is therefore a site interconversion of the molecule in the supercage.

The interpretation in terms of a site interchange is supported by the observation of infrared product bands that do not exhibit a thermal effect. One such band is the 1365 $cm^{-1}$ absorption of allyl hydroperoxide. Spectra taken 360, 1360, and 2840 ms after the laser pulse are shown in Figure 2. Data from 2160 pulses were averaged. The intensity of this band is the same at all three delay times. As a $CH_3$ bending mode,[1b] the 1365 $cm^{-1}$ absorption is indeed expected to be much less sensitive to a change in the local zeolite environment than an OH mode. The latter is engaged in strong H bonding to the wall oxygens as indicated by the large red shift of 500 $cm^{-1}$ of the $\nu$(OH) absorption compared to the gas phase.[23] Figure 2 indicates that the growth of the allyl hydroperoxide is complete within 330 ms after the laser pulse. Our goal was to find out whether this result is supported by the growth behavior of all other product infrared absorptions.

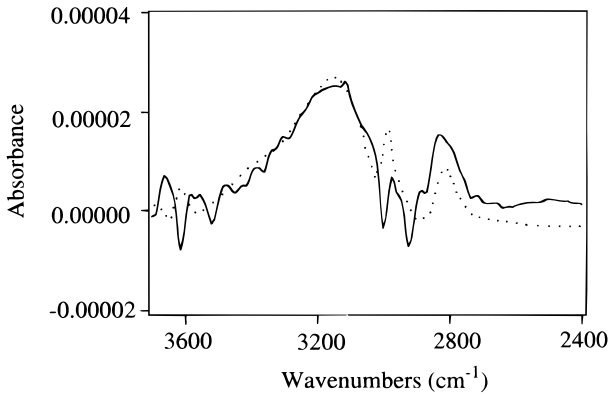


**Figure 3.** Rapid scan FT-IR spectra of the OH stretch absorption of the hydroperoxide product recorded 2760 ms after the laser pulse (solid line). In this experiment, the result of 380 laser pulses was averaged. The wide-dotted line represents the average growth per pulse obtained by dividing the difference of the static spectra before and after the rapid scan experiment by the number of laser pulses.

**2. Millisecond Spectrum of the Full Infrared Range.** To minimize or even eliminate the laser-induced thermal effect on the infrared product absorptions, two methods were explored. The simplest approach is to reduce substantially the number of laser flashes used for averaging since the magnitude of the thermal effect scales with the amount of accumulated product. Indeed, when averaging just 380 laser pulses (three consecutive experiments), the 2760 ms spectrum of the allyl hydroperoxide OH stretch absorption showed no thermal effect, as can be seen from Figure 3 (full trace). The wide-dotted curve is the difference in the static spectra recorded before and after the time-resolved experiment divided by the number of laser pulses; hence, it reflects the average growth per pulse. The good agreement in the OH stretching region of this static spectrum (which is free of thermal effects) and the growth after 2760 ms implies that the time-resolved spectrum is not influenced by any thermal effect. (Any such effect would reduce the signal relative to the static spectrum.) This means that the hydroperoxide product growth is complete within 2.8 s after the laser pulse. On the other hand, spectra at shorter times after the pulse still showed a smaller signal. Hence, the question remained whether thermal effects persisted during the first 2 s after the excitation pulse.

Recording of the true product absorbance in the first few hundred milliseconds after the pulse required use of a different experimental approach. The basic idea was to conduct the time-resolved experiment in the presence of a sufficiently large background of 2,3-dimethyl-3-hydroperoxy-1-butene so that the thermal laser effect on the product bands was unchanged during the entire run. If two pulsed laser runs were performed, one with DMB and $N_2$ and the other with DMB and $O_2$ in the zeolite, the difference of $O_2$ and $N_2$ spectra at a given time delay would reveal the real absorbance growth of the product since the thermal effects would cancel out. Step-by-step procedure included irradiation of the olefin and $O_2$-loaded pellet with visible light to accumulate hydroperoxide product, followed by removal of $O_2$ and replacement by 125 Torr of $N_2$. Under this pressure the $N_2$ concentration was the same as that of $O_2$ at 800 Torr.[7] The rapid scan run (3700−2300 $cm^{-1}$) was conducted at 173 K with 380 laser pulses and furnished averaged spectra at 330, 1280, and 2760 ms delay which showed the thermal effect only. Then, $N_2$ was replaced by $O_2$ and the time-resolved experiment repeated. Differences of corresponding $O_2$ and $N_2$ spectra resulted in the time-resolved traces shown in Figure 4 for the OH stretching region and in Figure 5 for the fingerprint region.

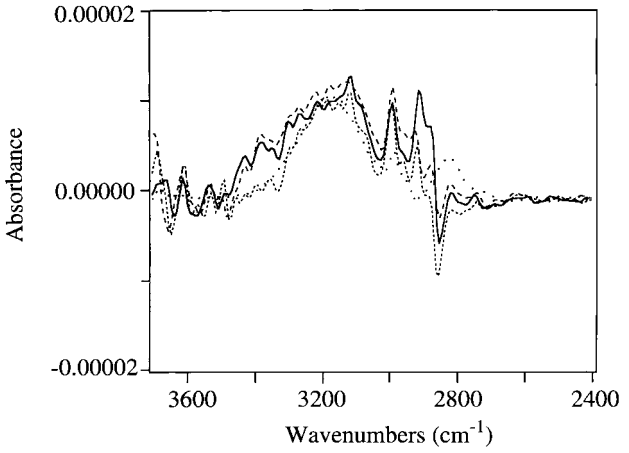


**Figure 4.** Rapid scan FT-IR spectra of the DMB + $O_2$ photoreaction in the OH stretch region. The traces at 330 ms (solid line), 1280 ms (dotted line), and 2760 ms (dashed line) were obtained by subtraction of corresponding time-resolved spectra of runs taken with $N_2$ from those obtained with $O_2$ in order to eliminate thermal effects. The static spectrum (wide-dotted line) is the difference of spectra before and after the rapid scan run ratioed against the number of laser pulses.

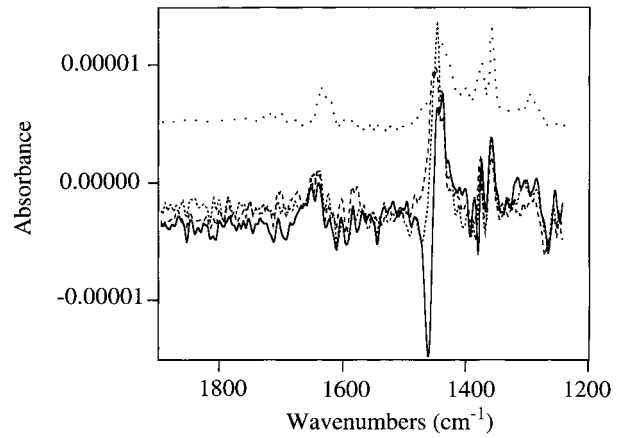


**Figure 5.** Rapid scan FT-IR spectra of the DMB + $O_2$ reaction in the fingerprint region. Traces are spectra with time delays of 360 ms (solid line), 1360 ms (dotted line), and 2840 ms (dashed line). Spectra were obtained by the procedure described in the caption of Figure 4. Thermal effects of the intense 1464 $cm^{-1}$ DMB absorption are not completely compensated for by the $O_2-N_2$ subtraction method.

At all three time delays, the broad allyl hydroperoxide OH stretching absorption is the same within uncertainties and agrees well with that of the static spectrum. Similarly, no significant differences can be discerned from the corresponding time-resolved spectra in the 2000−1200 $cm^{-1}$ region. The two product absorptions at 1365 $cm^{-1}$ ($CH_3$ bending mode) and 1650 $cm^{-1}$ (C═C stretch)[1b] show this especially clearly because these are free of overlap with reactant bands. Product absorptions at 1384, 1407, and 1450 $cm^{-1}$ (all $CH_3$ bending modes) overlap with decreasing DMB bands at 1385, 1400, and 1464 $cm^{-1}$, respectively.[1b] Nevertheless, their behavior is consistent with a constant concentration of allyl hydroperoxide at all three time delays. We conclude that upon photolysis of the olefin·$O_2$ pairs with a 150 ms pulse at 173 K there is no subsequent dark growth on the hundreds of milliseconds and seconds time scale.

**3. Implication of the Results.** The finding that at −100 °C the growth of the allyl hydroperoxide product is complete upon termination of the 150 ms laser pulse is no surprise in light of the previously proposed mechanism. The initial step following photochemical preparation of the charge-transfer state is proton transfer from the alkene radical cation to $O_2^-$ to form the allyl radical and HOO radical (Scheme 1 of ref 1b). The proton transfer is expected to be very fast (nanoseconds or faster) because these hydrocarbon radical cations are known to be very strong acids.[24,25] Similarly, the subsequent, barrier-free combination of allyl and HOO radicals is most probably geminate.

A crucial question is whether the product molecules are able to escape from the original supercage during the laser pulse, i.e., whether there is turnover of reactants and products within one and the same pulse. No measurements of diffusion coefficients have been reported for allyl hydroperoxides or similar polyfunctional organics in zeolites. However, we can make an order of magnitude estimate based on diffusion coefficients of molecules in $Na^+$-exchanged faujasites that contain at least one of the functionalities of 2,3-dimethyl-3-hydroperoxy-1-butene. The OH group is the most strongly interacting group of the allyl hydroperoxide with the zeolite as indicated by a 500 $cm^{-1}$ red shift of the OH stretch. Therefore, it is likely to influence the diffusion rate of the product more than any other factor, which makes the known diffusion coefficient of $CH_3OH$ a reasonable point of departure. Measurements in NaX with infrared, pulsed field gradient NMR, and zero-length column methods allow an estimate of the self-diffusion coefficient of $3 \times 10^{-14}$ $m^2$ $s^{-1}$ at 173 K.[26,27] This value has been extrapolated using the Arrhenius law from experiments in the range from 20 to 160 °C, which gave an activation energy[26] of 12 kJ $mol^{-1}$. The Arrhenius equation is typically found to be a good approximation of the temperature dependence of the diffusion coefficient of small hydrocarbons in zeolites. Although experimental studies of the temperature dependence are usually limited to ranges above room temperature,[28] model calculations suggest that the Arrhenius behavior of diffusion coefficients may extend to temperatures as low as 100 K.[29]

The vinyl group influences the diffusion of the allyl hydroperoxide product through $\pi$ interaction with the $Na^+$ ions.[28] The effect on the diffusion coefficient can be estimated by comparing the diffusion rates of $CH_2$═$CH_2$ and $CH_4$ in zeolite NaY at 173 K. The self-diffusion coefficient of $CH_4$ in NaY at 173 K is known from quasi-elastic neutron scattering[30] as $3 \times 10^{-9}$ $m^2$ $s^{-1}$, a value that agrees well with pulsed field gradient NMR measurements in NaX.[31] The diffusion coefficient of ethylene based on NMR work[32] is $3 \times 10^{-12}$ $m^2$ $s^{-1}$. Hence, the presence of the vinyl group is expected to reduce the diffusion coefficient by a factor of $10^3$. Furthermore, we have to account for the fact that the product molecule has seven carbons, not just two. The effect of the carbon number on diffusivities and diffusional activation energies has been reported for alkanes in NaX.[33] Taking activation energies 8.4 kJ $mol^{-1}$ ($C_2H_6$) and 13.0 kJ $mol^{-1}$ ($C_7H_{16}$) and preexponential factors $5 \times 10^{-7}$ $m^2$ $s^{-1}$ ($C_2H_6$) and $1.6 \times 10^{-7}$ $m^2$ $s^{-1}$ ($C_7H_{16}$), we calculate that the size of the hydrocarbon skeleton causes a lowering of the diffusion coefficient by a factor of 80 at 173 K. With all factors taken into account, the estimated diffusion coefficient of 2,3-dimethyl-3-hydroperoxy-1-butene in zeolite NaY at 173 K is $4 \times 10^{-19}$ $m^2$ $s^{-1}$.

The lowest possible diffusion coefficient that a guest molecule needs to have in order to escape a supercage within 150 ms can be calculated from the Einstein relation[34]

$$\langle r^2(t) \rangle = 6Dt \qquad (1)$$

The mean-square displacement $r$ in this case is equal to the 13 Å center-to-center separation of two adjoining supercages.[7] According to eq 1, the diffusion coefficient $D$ must be $2 \times 10^{-18}$ $m^2$ $s^{-1}$ or larger in order for the product molecule to reach

a neighboring supercage within $t = 150$ ms. Because of the small volume of the supercage, turnover of even a few hydroperoxides would only be possible if product molecules move several cages away from the original cage during this time interval, requiring a diffusion coefficient of at least $10^{-17}$ $m^2\ s^{-1}$. This is inconsistent with our estimate of $4 \times 10^{-19}$ $m^2\ s^{-1}$ for the diffusion coefficient of 2,3-dimethyl-3-hydroperoxy-1-butene. We conclude that the diffusion coefficient of the hydroperoxide is too low to permit turnover of products in a given supercage within the duration of the laser pulse. Therefore, the number of product molecules per pulse is equal to the number of cages that participated in reaction induced by that pulse. Rapid scan spectroscopy of the reaction required averaging over hundreds of laser shots. However, since the millisecond FT-IR spectra reveal that there is no growth of product in the dark periods between laser pulses, the infrared absorbance growth displayed in Figures 4 and 5 represents the number of supercages participating in reaction induced by one pulse. On the basis of the observed absorbance growth of the 1365 $cm^{-1}$ product band (Figure 5), its extinction coefficient,[2] and the number of supercages of the NaY pellet used, we calculate that $1.4 \times 10^{-10}$ mol or 0.006% of all supercages participate in reaction per pulse.

To estimate a lower limit for the number of participating supercages when we irradiate the zeolite with hundreds or even thousands of photolysis pulses, we have to know whether the dark periods between the pulses influence the produce yield. If the fraction of reactive cages was small, we would expect higher yields if turnover of reactant and product molecules occurs in these cages during the dark periods between pulses. To address this question, we loaded a NaY pellet with DMB and $O_2$ and exposed it to 2400 photolysis pulses of 150 ms duration (500 mW power) at 173 K. The dark period between the pulses was 1.35 s; hence, the experiment lasted 60 min. Then, the photolysis was repeated with the same total number of photons, but this time by irradiating continuously (6 min at 500 mW). Spectra were recorded after 54 min in the dark in order to reach the same total duration as in the pulsed experiment. Infrared difference spectra revealed the same cumulative allyl hydroperoxide growth in pulsed and continuous experiment within 4% uncertainty. The error estimate reflects the fluctuation of product growth after correcting for the monotonic decrease of the product yield due to reactant depletion.

This experimental finding imposes a lower limit on the number of supercages that participate in photoreaction. This number cannot be lower than the number of product molecules generated during a photolysis period equal to the time needed for the product to diffuse away from the parent cage. Removal of the allyl hydroperoxide from the original cage is essential if turnover is yield-limiting. The hydroperoxide is by far the least mobile species in the zeolite; hence, its diffusion coefficient would dictate the turnover time. With a constant of $4 \times 10^{-19}$ $m^2\ s^{-1}$, we estimate on the basis of eq 1 a minimum turnover time of 1 s. Since there are 0.006% cages participating per 150 ms pulse, 0.04% of all supercages take part in reaction during 1 s of continuous photolysis. The product yields of pulsed and continuous experiments are the same within 4%; hence, at most 1/25 of all reactive supercages are participating in reaction during 1 s of continuous photolysis. This is because it takes on the order of 1 s to replenish a cage in which reaction has taken place. Therefore, in the continuous experiment, 1/25 of all reactive cages are not available for photoreaction most of the time. In the pulsed experiment, by contrast, the 1.35 s dark periods allow essentially complete turnover of product and reactants between pulses, resulting in a 4% higher product yield. Hence, we estimate that at least 1% ($= 0.04\% \times 25$) of all NaY supercages participate in photoreaction.

Zeolite defects that might be capable of promoting photooxidation are Lewis acid sites (electron-deficient framework Al or extraframework Al species) or radical sites.[35] There are numerous reports confirming that zeolite NaY is free of such sites,[36] and we are not aware of any ESR spectroscopic signals observed in pure NaY crystallites. ESR work by Stamires and Turkevich puts the detection limit for radical sites at $3 \times 10^{15}$ spins per gram of NaY. This means that at most $8 \times 10^{-6}$ of all NaY supercages contain a radical defect site.[37] The standard method for Lewis acid site detection is loading of the zeolite with a base such as pyridine or triphenylamine. Determination of Lewis acid sites by loading of triphenylamine indicated a detection limit of $1 \times 10^{17}$ spins per gram of NaY; i.e., at most 0.0003 of all supercages have a Lewis acid site.[38] In our own previous attempts to detect Lewis acid sites in NaY by the pyridine method,[1f] we did not observe any infrared absorption at the characteristic frequency of 1450 $cm^{-1}$.[39] With an absorbance detection limit of $3 \times 10^{-4}$ au and an extinction coefficient of 1200 L $mol^{-1}$ $cm^{-1}$ for the 1450 $cm^{-1}$ pyridine $\nu$(C═C) absorption in zeolite,[40,41] we calculate that less than 0.0001 of all NaY supercages have a Lewis acid site. We conclude that the upper limit for Lewis acid or radical sites in NaY lies 2−3 orders of magnitude below our lower limit of cages participating in reaction. Therefore, such defects are not responsible for the visible light-induced olefin photooxidation.

## IV. Conclusions

The rapid scan FT-IR study of olefin photooxidation in a zeolite reported here demonstrates that time-resolved infrared spectroscopy of an irreversible reaction in a solid matrix is feasible despite the challenge posed by the accumulating product that cannot be removed from the area probed by the infrared beam. Because of its broad probing range, time-resolved FT-infrared spectroscopy is expected to become a useful tool for elucidating mechanisms of photochemical reactions in zeolites and other microporous solids.

The millisecond FT-IR spectra of the visible light-induced oxidation of 2,3-dimethyl-2-butene by $O_2$ in zeolite NaY at low temperature furnish direct evidence against any significant role of defect sites in the mechanism. This indicates that the sole physical property of the NaY supercage, namely the high electrostatic field around the exchangeable cations, is responsible for the low-energy photochemical path of this mild hydrocarbon oxidation.

**Acknowledgment.** This work was supported by the Director, Office of Energy Research, Office of Basic Energy Sciences, Chemical Sciences Division of the U.S. Department of Energy, under Contract No. DE-AC03-76SF00098.

## References and Notes

(1) (a) Blatter, F.; Frei, H. *J. Am. Chem. Soc.* **1993**, *115*, 7501. (b) Blatter, F.; Frei, H. *J. Am. Chem. Soc.* **1994**, *116*, 1812. (c) Sun, H.; Blatter, F.; Frei, H. *J. Am. Chem. Soc.* **1994**, *116*, 7951. (d) Blatter, F.; Sun, H.; Frei, H. *Catal. Lett.* **1995**, *35*, 1. (e) Blatter, F.; Sun, H.; Frei, H. *Chem. Eur. J.* **1996**, *2*, 385; *Angew. Chem., Int. Ed. Engl.* **1996**, *35*. (f) Sun, H.; Blatter, F.; Frei, H. *J. Am. Chem. Soc.* **1996**, *118*, 6873. (g) Frei, H.; Blatter, F.; Sun, H. *CHEMTECH* **1996**, *26*, 24. (h) Sun, H.; Blatter, F.; Frei, H. In *Heterogeneous Hydrocarbon Oxidation;* Oyama, S. T., Warren, B. K., Eds.; ACS Symposium Series No. 638; American Chemical Society: Washington, DC, 1996; p 409. (i) Sun, H.; Blatter, F.; Frei, H. *Catal. Lett.* **1997**, *44*, 247. (j) Blatter, F.; Sun, H.; Vasenkov, S.; Frei, H. *Catal. Today*, in press.

(2) Blatter, F.; Moreau, F.; Frei, H. *J. Phys. Chem.* **1994**, *98*, 13403.

(3) Vasenkov, S.; Frei, H. *J. Phys. Chem. B* **1997**, *101*, 4539.

(4) Evans, D. F. *J. Chem. Soc.* **1953**, 345.
(5) Tsubomura, H.; Mulliken, R. S. *J. Am. Chem. Soc.* **1968**, *82*, 5966.
(6) Mulliken, R. S.; Person, W. B. *Molecular Complexes*; Wiley: New York, 1969; Chapter 14.
(7) Breck, D. W. *Zeolite Molecular Sieves: Structure, Chemistry and Use*; Wiley: New York, 1974.
(8) Barrachin, B.; Cohen de Lara, E. *J. Chem. Soc., Faraday Trans. 2* **1986**, *82*, 1953.
(9) Smudde, G. H.; Slager, T. L.; Coe, C. G.; MacDougall, J. E.; Wiegel, S. J. *Appl. Spectrosc.* **1995**, *49*, 1747.
(10) Angell, C. L.; Schaffer, P. C. *J. Phys. Chem.* **1966**, *70*, 1413.
(11) Zecchina, A.; Bordiga, S.; Lamberti, C.; Spoto, G.; Carnelli, L. *J. Phys. Chem.* **1994**, *98*, 9577.
(12) Coope, J. A. R.; Gardner, C. L.; McDowell, C. A.; Pelman, A. I. *Mol. Phys.* **1971**, *21*, 1043.
(13) Sugihara, H.; Shimokoshi, K.; Yasumori, I. *J. Phys. Chem.* **1977**, *81*, 669.
(14) Spackman, M. A.; Weber, H. P. *J. Phys. Chem.* **1988**, *92*, 794.
(15) Huang, Y. Y.; Benson, J. E.; Boudart, M. *Ind. Eng. Chem. Fundam.* **1969**, *8*, 346.
(16) Dempsey, E. In *Molecular Sieves*; Society of Chemical Industry: London, 1968; p 293.
(17) Preuss, E.; Linden, G.; Peuckert, M. *J. Phys. Chem.* **1985**, *89*, 2955.
(18) White, J. C.; Nicholas, J. B.; Hess, A. C. *J. Phys. Chem. B* **1997**, *101*, 590.
(19) Blatter, F.; Frei, H., to be submitted for publication.
(20) Sloan, J. J.; Kruus, E. J. In *Time-Resolved Spectroscopy;* Clark, R. J. H., Hester, R. E., Eds.; Wiley: New York, 1989; Vol. 18, p 219.
(21) Sun, H.; Frei, H. *J. Phys. Chem. B* **1997**, *101*, 205.
(22) Van de Hulst, H. C. *Light Scattering by Small Particles*; Wiley: New York, 1957; p 267.
(23) Gleason, W. S.; Broadbent, A. D.; Whittle, E.; Pitts, Jr., J. N. *J. Am. Chem. Soc.* **1970**, *92*, 2068.
(24) Anderson, D. R.; Bierbaum, V. M.; Depuy, C. H.; Grabowski, J. J. *Int. J. Mass Spectrom. Ion Phys.* **1983**, *52*, 65.
(25) Hammerich, O.; Parker, V. D. *Adv. Phys. Org. Chem.* **1984**, *20*, 55.
(26) Grenier, P.; Meunier, F.; Gray, P. G.; Kärger, J.; Xu, Z.; Ruthven, D. M. *Zeolites* **1994**, *14*, 242.
(27) Brandani, S.; Ruthven, D. M.; Kärger, J. *Zeolites* **1995**, *15*, 494.
(28) Kärger, J.; Ruthven, D. M. *Diffusion in Zeolites*; Wiley: New York, 1992; Chapters 12 and 13.
(29) Auerbach, S. M.; Henson, N. J.; Cheetham, A. K.; Metiu, H. I. *J. Phys. Chem.* **1995**, *99*, 10600.
(30) Jobic, H.; Bee, M.; Kearley, G. J. *J. Phys. Chem.* **1994**, *98*, 4660.
(31) Kärger, J.; Pfeifer, H.; Rauscher, M.; Walter, A. *J. Chem. Soc., Faraday Trans. 1* **1980**, *76*, 717.
(32) Burmeister, R.; Boddenberg, B.; Verfürden, M. *Zeolites* **1989**, *9*, 318.
(33) Reference 28, p 436.
(34) Reference 28, p 25.
(35) Mortier, W. J.; Schoonheydt, R. A. *Prog. Solid State Chem.* **1985**, *16*, 33.
(36) Ward, J. W. In *Zeolite Chemistry and Catalysis*; Rabo, J. A., Ed.; ACS Symposium Series No. 171; American Chemical Society: Washington, DC, 1976; p 118, and references therein.
(37) Stamires, D. N.; Turkevich, J. *J. Am. Chem. Soc.* **1964**, *86*, 757.
(38) Stamires, D. N.; Turkevich, J. *J. Am. Chem. Soc.* **1964**, *86*, 749.
(39) Ward, J. W. *J. Catal.* **1968**, *10*, 34.
(40) Reference 36, p 251.
(41) Borade, R. B.; Adnot, A.; Kaliaguine, S. *J. Chem. Soc., Faraday Trans.* **1990**, *86*, 3949.